Upper mantle seismic discontinuities

Peter M. Shearer

Institute of Geophysics and Planetary Physics, Scripps Institution of Oceanography, University of California, San Diego, La Jolla, California

The upper mantle seismic discontinuities provide important constraints on models of mantle composition and dynamics. New observations of reflected and converted phases from the discontinuities have made possible more detailed measurements of discontinuity structure than are provided by traditional analyses of refracted waveforms. This paper reviews seismic observations of discontinuity properties, including their depth, topography, sharpness, and amplitude. Topography on the 410- and 660-km discontinuities is largely uncorrelated at global scales, and the *660* topography is significantly larger in peak-to-peak amplitude. The positions of subduction zones are correlated with depressions in the 660-km discontinuity, consistent with tomography results indicating the presence of large cold (fast) regions deep in the transition zone. A significant fraction of the velocity increases near 410 and 660 km occur over a depth interval less than 5 km; the 520-km reflector is more diffuse and appears to occur over a 10 to 50 km depth interval. The magnitude of the velocity and density increases across the discontinuities are poorly constrained by many seismic observations; they are currently best resolved from measurements of the amplitudes of reflected phases.

1. INTRODUCTION

The properties of the seismic discontinuities in the upper mantle provide an important link between mineral physics experiments and seismic observations. These properties include the discontinuity depths and topography, the size of the velocity and density increases, and the sharpness of the boundaries. In addition, deriving accurate maps of discontinuity topography depends upon applying corrections based on tomographic images of upper mantle velocity structure. Thus, this subject is well suited to this special volume.

Studies of the upper mantle discontinuities have a long and distinguished history in seismology that I will not attempt to review comprehensively here. Rather, I will summarize the best current constraints on the discontinuity properties, and point out the approximate uncertainties in the various types of measurements that have been made. My focus will be on the well-established discontinuties of the mantle transition zone at mean depths near 410, 520, and 660 km. The term "discontinuity" has traditionally been applied to these features, although they may involve steep velocity gradients rather than first-order discontinuities in seismic velocity. Discontinuities at other depths have often been postulated, but there is as yet little consensus on the global existence of these features, and their aver-

Earth's Deep Interior: Mineral Physics and Tomography From the Atomic to the Global Scale
Geophysical Monograph 117

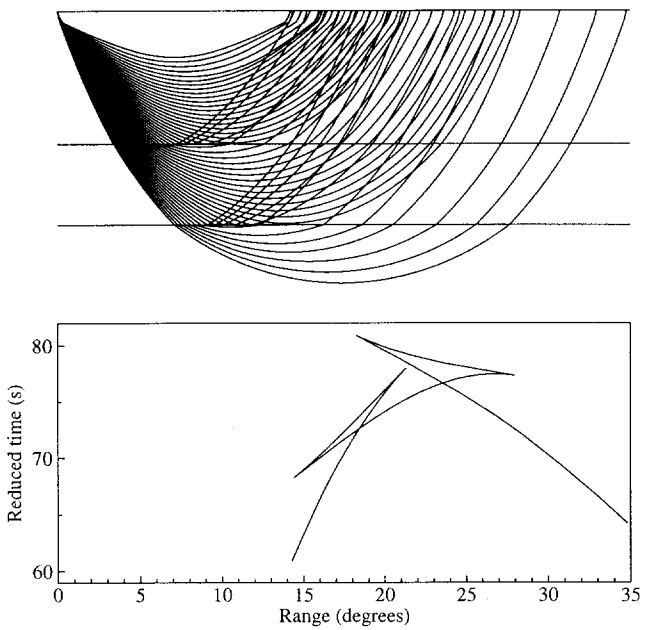

Figure 1. P wave ray paths and travel times predicted by the IASP91 velocity model. A reducing velocity of 10 km/s is used for the lower plot. The sharp velocity increases at 410 and 660 km produce two triplications in the travel time curve, centered at 20° to 25° range. The first arrivals alone do not provide much information on details of the velocity structure near the discontinuities; it is the later arrivals that give the best constraints on discontinuity structure.

age properties are known so poorly, that their relevance to mineral physics or tomography at this point remains uncertain.

For convenience, I will refer to the discontinuities as the *410*, *520*, and *660*, although their actual depths may vary. It is now generally accepted that most, if not all, of the velocity and density jumps near 410 and 660 km result from phase changes in olivine and other minerals. The 520-km discontinuity has proven more controversial and its necessity has sometimes been questioned [e.g., *Bock*, 1994], but the bulk of the seismic evidence now favors an enhanced velocity gradient near 520 km that may be associated with the β-olivine to γ-spinel phase change [e.g., *Rigden et al.*, 1991].

2. OBSERVING UPPER MANTLE DISCONTINUITIES

Upper mantle discontinuities can best be detected from analysis of seismic waves that bottom near the discontinuities (refraction seismology), or, more recently, through study of secondary seismic phases reflected or converted at the interfaces. Figure 1 shows the triplications in the travel times near 20° range that are characteristic of the upper mantle discontinuities, as predicted by the IASP91 velocity model [*Kennett*, 1991]. These triplications can be observed in both P and S waves. Older studies of the triplications analyzed the timing (and sometimes the slopes, if array data were available) of the different branches of the travel-time curves. However, because the first arriving waves do not directly sample the discontinuities, and the onset times of secondary arrivals are difficult to pick accurately, these data are best examined using synthetic seismogram modeling. The goal is to find a velocity-depth profile that predicts theoretical seismograms that match the observed waveforms. This inversion procedure is difficult to automate, and most results have been obtained using trial-and-error forward modeling approaches [e.g., *Grand and Helmberger*, 1984; *Walck*, 1984; *Ryberg et al.*, 1998].

An advantage of this type of modeling is that it often provides a complete velocity versus depth function extending from the surface through the transition zone. Thus, in principle, some of the tradeoffs between shallow velocity structure and discontinuity depth that complicate analysis of reflected and converted phases (see below) are removed. However, significant ambiguities remain. It is difficult to derive quantitative error bounds on discontinuity depths and amplitudes from forward modeling results. Tradeoffs are likely between the discontinuity properties and velocities immediately above and below the discontinuities—regions that are not sampled with first-arrival data. The derived models tend to be the simplest models that are found to be consistent with the observations. In most cases, the *410* and *660* discontinuities are first-order velocity jumps, separated by a linear velocity gradient. However, velocity increases spread out over 10 to 20 km depth intervals would produce nearly identical waveforms (except in the special case of pre-critical reflections, see below), and subtle differences in the velocity gradients near the discontinuities could be missed. The data are only weakly sensitive to density; thus density, if included in a model, is typically derived using a velocity versus density scaling relationship.

An alternative approach to investigating upper mantle discontinuity depths involves the study of minor seismic phases that result from reflections and phase conversions at the interfaces. These can take the form of P or S topside and bottomside reflections, or P-to-S and S-to-P converted phases. Typically these phases are too weak to observe clearly on individual seismograms, but stacking techniques (the averaging of results from many records) can be used to enhance their visibility. Analysis and interpretation of these data have many

similarities to techniques used in reflection seismology.

The most important of the upper mantle discontinuity phases are illustrated in Figures 2 and 3 and include:

(1) Precursors to $P'P'$ ($PKPPKP$) resulting from underside reflections [e.g, *Engdahl and Flinn*, 1969; *Whitcomb and Anderson*, 1970; *Husebye et al.*, 1977; *Nakanishi*, 1986, 1988, 1989; *Davis et al.*, 1989; *Benz and Vidale*, 1993; *Le Stunff et al.*, 1995; *Xu et al.*, 1998; 1999]. These are seen at high frequencies, often on individual seismograms, and provide the best current constraints regarding the sharpness of the discontinuities. The precursors are denoted $P'dP'$, where d is the discontinuity depth.

(2) P-to-SV conversions from discontinuities beneath the receivers [e.g., *Vinnik*, 1977; *Vinnik et al.*, 1983; *Kind and Vinnik*, 1988; *Paulssen*, 1985, 1988; *Shearer*, 1990, 1991; *Stammler et al.*, 1991; *Petersen et al.*, 1993; *Gurrola*, 1995; *Bostock*, 1996; *Vinnik et al.*, 1996; *Shen et al.*, 1996, 1998; *Chen et al.*, 1997; *Kosarev et al.*, 1999]. These can be analyzed in the same way as crustal receiver functions and provide estimates for discontinuity depths beneath individual seismic stations. If closely spaced stations are available, it may be possible to use these data to resolve small-scale topography on the discontinuities [e.g., *Li et al.*, 1998; *Dueker and Sheehan*, 1997, 1998]. These phases are denoted Pds, where d is the discontinuity depth.

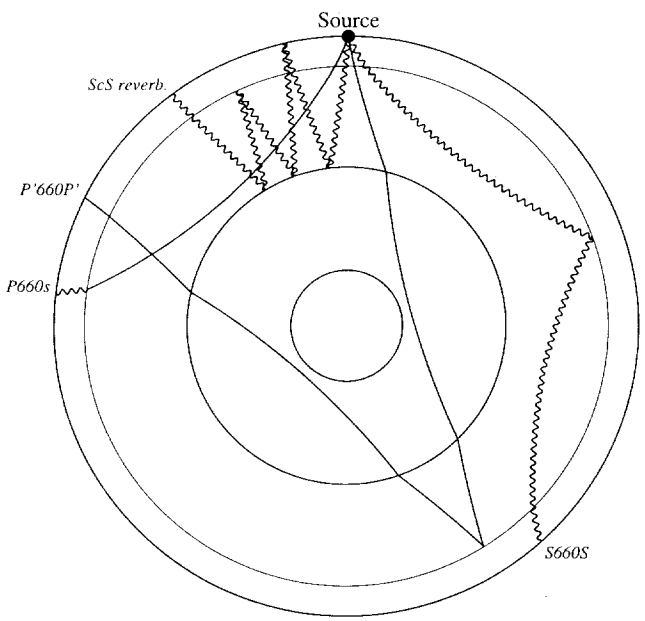

Figure 2. Example ray paths for discontinuity phases resulting from reflections or phase conversions at the 660-km discontinuity, computed using the IASP91 velocity model. P waves are shown as smooth lines, S waves as wiggly lines. The ScS reverberations include a large number of top- and bottom-side reflections, only a single example of which is plotted.

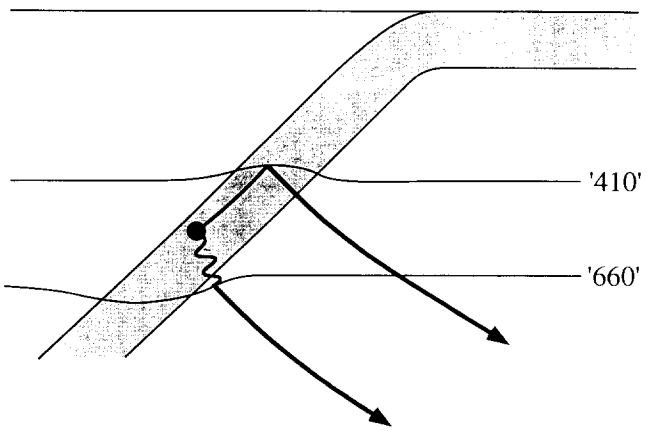

Figure 3. A cartoon showing example ray paths for near-source reflections and phase conversions from deep earthquakes in subducting slabs. P waves are shown as smooth lines, S waves as wiggly lines. The underside P reflection from the 410-km discontinuity, and the S-to-P conversion from the 660-km discontinuity are plotted.

(3) Precursors to SS resulting from underside reflections, seen in global data at long-periods [e.g., *Shearer*, 1991, 1993, 1996; *Shearer and Masters*, 1992; *Petersen et al.*, 1993; *Gossler and Kind*, 1995; *Lee and Grand*, 1996; *Flanagan and Shearer*, 1998a, *Gu and Dziewonski*, 1998]. These data provide the best constraints on the large-scale topography on the discontinuities, as the widely distributed SS bouncepoints have nearly complete global coverage. The precursors are termed SdS, where d is the reflector depth. Recently long-period PP precursors have also been analyzed [e.g., *Estabrook and Kind*, 1996; *Flanagan and Shearer*, 1999; *Shearer and Flanagan*, 1999] which provide additional constraints on 410 topography and the velocity and density jumps across the 410- and 660-km discontinuities.

(4) Topside and bottomside reflections from the discontinuities that arrive between long-period ScS surface reverberations [e.g., *Revenaugh and Jordan*, 1987, 1989, 1991a, 1991b; *Revenaugh and Sipkin*, 1994; *Katzman et al.*, 1998]. These can be used to estimate average discontinuity depths and amplitudes along 10° to 50° long regional paths.

(5) Near-source S-to-P conversions from deep events that arrive in the P coda [e.g., *Faber and Müller*, 1980, 1984; *Barley et al.*, 1982; *Bock and Ha*, 1984; *Richards and Wicks*, 1990; *Vidale and Benz*, 1992; *Wicks and Richards*, 1993; *Yamazaki and Hirahara*, 1994; *Estabrook et al.*, 1994; *Niu and Kawakatsu*, 1995, 1997; *Collier and Helffrich*, 1997; *Castle and Creager*, 1997,

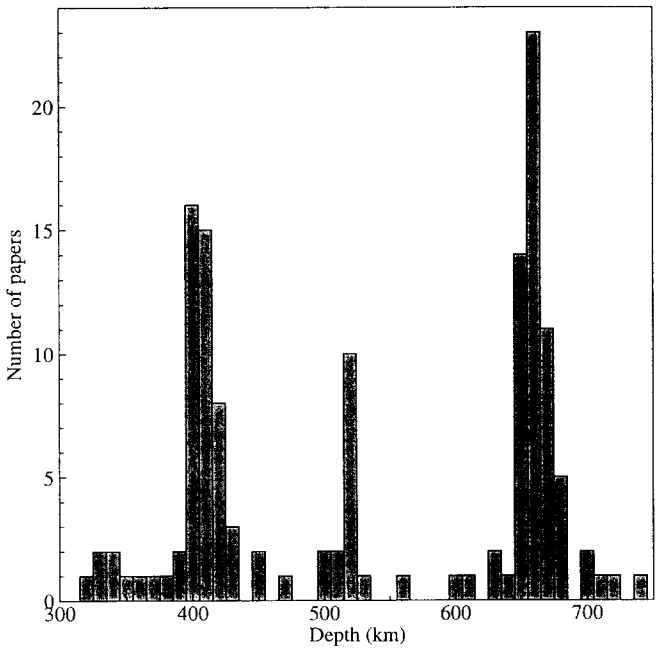

Figure 4. A histogram of upper-mantle discontinuity depths as cited in *Adams* [1971], *Barley et al.* [1982], *Baumgardt and Alexander* [1984], *Bock* [1988], *Bock and Ha* [1984], *Bock and Kind* [1991], *Brudzinski et al.* [1997] *Davis et al.* [1989], *Dey-Sarkar and Wiggins* [1976], *Drummond et al.* [1982], *Dueker and Sheehan* [1997], *Dziewonski and Anderson* [1981], *Engdahl and Flinn* [1969], *Faber and Müller* [1980, 1984], *Flanagan and Shearer* [1998], *Fukao* [1977], *Given and Helmberger* [1980], *Grand and Helmberger* [1984], *Graves and Helmberger* [1988], *Gurrola* [1995], *Gutowski and Kanasewich* [1974], *Hales* [1969], *Hales et al.* [1980], *Helmberger and Engen* [1974], *Helmberger and Wiggins* [1971], *Husebye et al.* [1977], *Johnson* [1967], *Kennett* [1991], *Kind and Vinnik* [1988], *Le Stunff et al.* [1995], *Lee and Grand* [1996], *LeFevre and Helmberger* [1989], *Leven et al.* [1981], *Li et al.* [1996], *Mechie et al.* [1993], *Nakanishi* [1986, 1988, 1989], *Niazi* [1969], *Niazi and Anderson* [1965], *Nolet* [1977], *Paulssen* [1985, 1988], *Pino and Helmberger* [1996], *Ram and Mereu* [1977], *Revenaugh and Jordan* [1991a], *Revenaugh and Sipkin* [1994], *Richards and Wicks* [1990], *Ryberg et al.* [1996, 1998], *Sacks et al.* [1979], *Shearer* [1991, 1993, 1996], *Simpson et al.* [1974], *Souriau* [1986], *Stammler et al.* [1991], *Vidale and Benz* [1992], *Vinnik* [1977], *Vinnik et al.* [1983], *Walck* [1984], *Wallace and Holt* [1988], *Whitcomb and Anderson* [1970], *Wiggins and Helmberger* [1973], *Zhang and Lay* [1993], and *Zhao and Helmberger* [1993].

1998]. These are useful for determining local depth estimates for the 660-km discontinuity in the vicinity of subducting slabs. This phase geometry has also been used to identify deeper scattering surfaces in the mid-mantle [e.g., *Niu and Kawakatsu*, 1997; *Kaneshima and Helffrich*, 1998; 1999; *Castle and Creager*, 1999]

(6) Near-source underside reflections from deep events that arrive as precursors to pP, sS and sP, and provide local depth estimates for the 410-km discontinuity near subducting slabs [e.g, *Vidale and Benz*, 1992; *Zhang and Lay*, 1993; *Ritsema et al.*, 1995; *Flanagan and Shearer*, 1998b; *Collier and Helffrich*, 1997].

In all cases, the timing of the arrivals provides direct constraints on discontinuity depths, although a reference velocity model must be assumed to convert the observed times to depths. While individual time measurements of these phases can be quite precise, uncertainties in the reference velocity model often limit the accuracy of the depth estimates. One advantage of these secondary phases is that they can provide more direct constraints on the amplitude of the discontinuities than analysis of refracted waves through the 20° triplications. In addition, many of the phases are sensitive to the impedance jump (impedance is the product of density and seismic velocity) at the discontinuity, so that, in principle, with enough different types of data, the velocity and density jumps can be separately determined.

3. AVERAGE DISCONTINUITY DEPTHS

Depth is the most precisely measured property of the upper mantle discontinuities. It is the agreement between the average discontinuity depths of about 415, 520 and 660 km and the experimentally observed pressures for phase changes in olivine that has provided the most generally accepted explanation for these features. The discontinuity depths give relatively direct measurements of *in situ* mantle temperatures, assuming pressure versus temperature results are available for the appropriate mineral phase changes.

A histogram of discontinuity depths as cited in 67 papers published since 1965 is shown in Figure 4. These depths were obtained using a variety of different approaches, including modeling of the 20° triplication and analyses of reflected and converted phases. Three distinct peaks near 410, 520 and 660 km are visible above the background "noise" level of discontinuity observations. The existence of the 410- and 660-km discontinuities has been well established for many years, but the necessity for a discontinuity near 520 km has been controversial. Observations of the *520* in refraction data come mainly from older analyses; most recent studies of the mantle triplications do not find evidence for a 520-km discontinuity [e.g., *Cummins*, 1992; *Jones et al.*, 1992], although several new analyses of long-range profiles from nuclear explosions across Eurasia have detected such a feature [*Mechie et al.*, 1993; *Ryberg et al.*, 1997]. More consistent evidence for a discontinuity near 520 km has come from observations of long-period

reflected phases [e.g., *Shearer*, 1990, 1991, 1996; *Revenaugh and Jordan*, 1991a; *Gossler and Kind*, 1995; *Gu and Dziewonski*, 1998].

Published upper mantle discontinuity depth estimates range from 390 to 430 km for the *410* discontinuity, 500 to 520 km for the *520* discontinuity, and 650 to 680 km for the *660* discontinuity. The mean reported discontinuity depths are close to 410, 520 and 660 km. Averaging a large number of different observations, while democratic, is probably not the best way to determine an accurate global average of the discontinuity depths. There are large differences in the quality of the data and modeling used in the different studies, and continental regions are sampled more often than oceanic regions. Some of the observed variations in depth may reflect regional differences, but much of the scatter may also be due to uncertainties in the modeling process. Interpretation of these results is complicated by the fact that sometimes the discontinuity depths are chosen to agree with a starting model, with adjustments made only if there is a significant misfit to the data.

Currently the best globally averaged depth estimates are obtained from analysis of SS precursor observations, due to the wide distribution of their sampling points. The most recent of these studies give mean depths for the discontinuities of 418, 515 and 660 km [*Flanagan and Shearer*, 1998a] and 411 and 654 km [*Gu and Dziewonski*, 1998]. For comparison, analyses of ScS reverberation data from paths around the western Pacific have indicated average depths of 414, 524 and 660 km [*Revenaugh and Jordan*, 1991a]. The differences between the SS precursor studies probably result mainly from the corrections applied for crust and upper mantle velocity structure. Both the *Flanagan and Shearer* [1998a] and *Gu and Dziewonski* [1998] studies attempted to correct for the effect of three-dimensional mantle structure as determined by recent global seismic tomography models. Uncertainties in these models, as well as a possible baseline shift problem in applying crustal corrections to velocity models [see *Flanagan and Shearer*, 1998a], are probably the leading sources of discrepancies in the discontinuity depth estimates. However, it is difficult to quantify these uncertainties with formal error bounds.

Because most of the uncertainties in the mantle velocity structure occur above 400 km, the transition zone thickness, d_{TZ}, as measured by the difference in depths between the *410* and *660* discontinuities, $d_{660} - d_{410}$, can be determined more reliably than the individual depths. Globally averaged thickness estimates obtained from recent SS precursor studies are 241 km [*Flanagan and Shearer*, 1998a] and 243 km [*Gu and Dziewonski*, 1998]. A value of d_{TZ} of 242 km is almost certainly within 1% of the true global average.

The meaning of these observed discontinuity depths is straightforward in the case of a sharp interface. If the velocity increase occurs linearly over a range in depth, then pulse broadening of the reflected pulse will occur, but in most cases the depth obtained from a long-period reflection will be close to the midpoint of the depth interval. However, if a non-linear velocity increase occurs, as models of mineral phase changes typically predict [e.g., *Helffrich and Bina*, 1994; *Solomatov and Stevenson*, 1994; *Helffrich and Wood*, 1996; *Stixrude*, 1997], then the reflectivity response is more complicated. In this case, a difference might exist between average long- and short-period reflector depths, but such a difference has not yet been established from observations. An obstacle to the possibility of making such an observation is the narrow bandwidth of most mantle discontinuity phases. For example, SS precursors are seen at long-periods but cannot be reliably observed at short periods, while $P'P'$ precursors are seen clearly only at relatively short periods. The frequency dependence in reflections arising from different velocity profiles is discussed at greater length in the section on discontinuity sharpness.

4. DISCONTINUITY TOPOGRAPHY

Just as absolute discontinuity depths provide a measurement of absolute mantle temperatures, discontinuity topography provides information on lateral variations in mantle temperatures. Discontinuity topography also introduces density variations that are an important constraint on geodynamic modeling of mantle flow. Differences in discontinuity depth estimates between different studies (see Figure 4) have long suggested that topography might exist on the discontinuities, but the first definitive evidence for topography came from ScS reverberation and SS precursor studies. *Revenaugh and Jordan* [1989, 1991a] found depth variations up to 20 km on the *410* and *660* discontinuities between different ScS reverberation paths, while *Shearer* [1991, 1993] and *Shearer and Masters* [1992] found evidence of global-scale topography on the discontinuities with variations of 30 to 40 km. The most comprehensive SS precursor studies to date are those of *Flanagan and Shearer* [1998a] and *Gu and Dziewonski* [1998], who analyze similar data sets of over 10,000 long-period seismograms from the global seismic networks.

In both studies, the data are binned by SS bounce-point location and averaged to improve the signal-to-

noise of the precursors. The timing of the precursors relative to the direct SS arrival is sensitive to both the discontinuity depth and the velocity structure of the crust and upper mantle, so corrections must be applied to account for surface topography, crustal thickness variations, and velocity heterogeneity in the upper mantle. The model of *Flanagan and Shearer* [1998a] is plotted in Plate 1. Good agreement exists between this model and that of *Gu and Dziewonski* [1998] for the *660* topography, but the models of *410* topography exhibit significant differences. The following characteristics are seen in both sets of models and appear to be reliable features of SS precursor observations:

(1) The amplitude of the large-scale *660* topography is significantly greater than the *410* topography. This is consistent with previous analyses [*Shearer*, 1991, 1993] and is one of the most robust features of mantle discontinuity observations. If the Clapeyron slope of the *410* phase change is comparable to or greater than the slope of the *660* phase change, as some mineral physics results suggest [e.g., *Bina and Helffrich*, 1994], this implies that the lateral temperature variations are larger at 660 km than at 410 km.

(2) The topographies of the *410* and *660* discontinuities are largely uncorrelated. In the recent past, some controversy has arisen over the question as to whether the discontinuity topography is observed to be correlated or anticorrelated [e.g., *Stammler et al.*, 1992; *Stammler and Kind*, 1992; *Revenaugh and Jordan*, 1992] (anticorrelation might be expected due to the opposite Clapeyron slopes of the *410* and *660* phase changes). This is a difficult test to perform, because the corrections for velocity structure above 410 km are so critical. Any inaccuracies in the application of these corrections will tend to induce artificial correlations in the discontinuity topography. Although the possibility cannot be excluded that a weak correlation or anticorrelation exists, the latest SS precursor results suggest that the global *410* topography cannot be accurately predicted from the *660* topography, at least at large scales.

(3) The power in the observed topography at long wavelengths is dominated by low spherical harmonic degree [e.g., *Gu and Dziewonski*, 1998]. This behavior is similar to that seen in recent mantle tomography models (3D seismic velocity inversions). However, the extent to which this result can be extrapolated to small scales is not yet clear, as there is evidence for significant discontinuity topography at scale lengths of hundreds of kilometers from studies of P-to-SV converted phases under continents [e.g., *van der Lee et al.*, 1994; *Dueker and Sheehan*, 1997, 1998; *Li et al.*, 1998], as well as observations of small-scale discontinuity structure near subducting slabs (see below).

(4) Depressions in the *660* discontinuity are correlated with subduction zones [*Shearer*, 1991; *Shearer and Masters*, 1992], consistent with the response of the *660* phase change to colder temperatures. The large scale of these features indicates that the thermal anomalies associated with the subducting slabs often become very broad near 660 km. In several cases, the positions of the *660* depressions coincide with fast, presumably cold, regions in the transition zone imaged in seismic tomography studies [e.g., *van der Hilst et al.*, 1991; *Fukao et al.*, 1992]. The lack of accompanying significant large-scale uplifts on the 410-km discontinuity suggests that these cold regions are confined to depths below 410 km.

The models of *410* topography produced by *Flanagan and Shearer* [1998a] and *Gu and Dziewonski* [1998] agree in peak-to-peak amplitude, but have significant differences in the patterns of highs and lows. Since both studies examine similar data sets of long-period SS precursors, the source for the discrepancy probably lies either in the processing method, or, more likely, in the corrections applied for crust and upper mantle structure. Resolving this difference will be necessary to address a current controversy regarding whether the observed topography of the *410* is significantly correlated with ocean-continent differences. *Gu and Dziewonski* [1998] identify such a correlation, suggesting that cold continental roots may extend below 400 km, but *Flanagan and Shearer* [1998b, 1999] find no significant correlation between *410* topography and continents. The latter position is supported, at least locally, by the recent analysis of P-to-SV conversions by *Li et al.* [1998], who map little change in the depth to the *410* across the eastern United States.

The resolution of the long-period SS precursor data can be approximated by the Fresnel zone at the SS bouncepoint, which is about 15° across [e.g., *Shearer*, 1991]. Smaller features cannot be reliably resolved, at least using the simple stacking approaches that have so far been applied to the data. Concern has been raised [*Neele et al.*, 1997; *Chaljub and Tarantola*, 1977] regarding the extent to which small-scale topography on the discontinuities might bias inferences of large-scale topography from SS precursors. This is an issue that needs further investigation, but the migration experiments of *Shearer et al.* [1999] suggest that this is not a serious problem. Small-scale topography on the discontinuities, such as might be anticipated near subducting slabs, is not resolved in SS precursor studies.

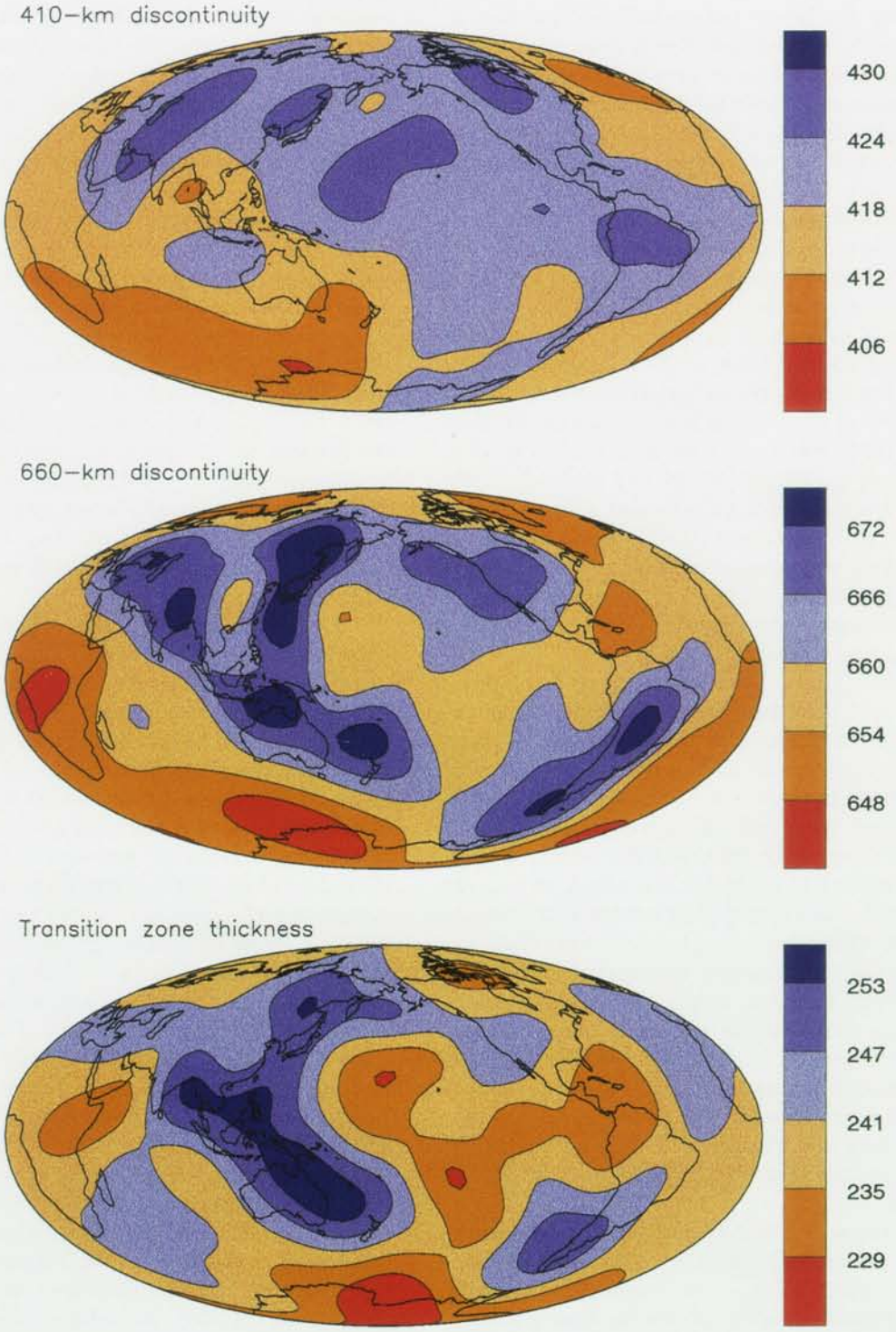

Plate 1. Model TOPOTZ of *Flanagan and Shearer* [1998a], showing large-scale topography on the *410* and *660* discontinuities and the transition zone thickness ($d_{TZ} = d_{660} - d_{410}$). These models are obtained from stacks of long-period SS precursors. The *410* discontinuity has peak-to-peak topography of about 22 km, compared to 38 km for the *660*. Depressions in the *660* are correlated with subduction zones.

However, finer resolution can be achieved by examining discontinuity phases that result from near-source or near-receiver reflections or phase conversions, since these phase geometries have much smaller Fresnel zones.

Records from deep subduction zone earthquakes are particularly interesting due to the variations in discontinuity depths that might be expected near the subducting slabs. Recent studies of underside reflections from the *410* discontinuity have indicated elevations of the *410* near subducting slabs of about 10 to 20 km [*Benz and Vidale*, 1992; *Ritsema et al.*, 1995; *Flanagan and Shearer*, 1998b] to as much as 60 km [*Collier and Helffrich*, 1997]. Recent studies of S-to-P conversions at the *660* discontinuity have indicated near slab depressions in the *660* of 20 to 30 km beneath Tonga [*Richards and Wicks*, 1990; *Niu and Kawakatsu*, 1995] and 40 to 60 km beneath Izu-Bonin [*Wicks and Richards*, 1993; *Collier and Helffrich*, 1997; *Castle and Creager*, 1998]. These results are not always directly comparable, due to differences in the velocity models assumed to compute the discontinuity depths and to uncertainties in the exact position of the sampling points with respect to the subducting slabs.

On the whole, these observations favor local elevations of the *410* and depressions of the *660* near the slabs that are consistent with the opposing Clapeyron slopes of the appropriate olivine phase changes. The local depressions in the *660* are somewhat deeper than the much larger scale regional depressions in the *660* seen in the SS precursor data. Notably absent are any direct observations of a kinetic depression of the *410* associated with the hypothesized existence of a wedge of metastable olivine extending below 410 km that may be related to deep earthquakes [for a review of this idea, see *Kirby*, 1996]. However, a very narrow wedge might be difficult to detect in the underside reflections [see discussion in *Flanagan and Shearer*, 1998b], so this is not definitive evidence against such a feature. Indirect evidence to support a metastable olivine wedge was presented by *Iidaka and Suetsugu* [1992] in an analysis of travel times of rays that travel up the subducting slab under Japan.

Under continents, P-to-SV converted phases can be used to map discontinuity depths with greater horizontal resolution than SS precursor studies. Potentially of great importance are recent results that point toward significant small-scale topography on the discontinuities. *Dueker and Sheehan* [1997, 1998] found 20 to 30 km of uncorrelated relief on the *410* and *660* discontinuities beneath the western United States over horizontal scale lengths of 200 to 300 km. Such roughness is consistent with the models inferred by *van der Lee et al.* [1994] to explain the lack of $P660s$ phases in data recorded by the NARS array across Europe. If such small-scale topography is indeed present, then significant horizontal variations in temperature and/or composition are implied at similar scale lengths.

5. DISCONTINUITY SHARPNESS

The most important evidence for the sharpness of the upper mantle discontinuities is provided by observations of short-period precursors to $P'P'$ [e.g, *Engdahl and Flinn*, 1969; *Whitcomb and Anderson*, 1970; *Nakanishi*, 1986, 1988, 1989; *Davis et al.*, 1989; *Benz and Vidale*, 1993; *Xu et al.*, 1998]. Underside reflections from both the *410* and *660* discontinuities are visible to maximum frequencies, f_{max}, of $\sim$1 Hz (sometimes slightly higher). The 520-km discontinuity is not seen in these data, even in data stacks with excellent signal-to-noise [*Benz and Vidale*, 1993], indicating that it is not as sharp as the other reflectors.

$P'P'$ precursor amplitudes are sensitive to the P impedance contrast across the discontinuities. Relatively sharp impedance increases are required to reflect high frequency seismic waves. This can be quantified by computing the reflection coefficients as a function of frequency for specific models. If simple linear impedance gradients are assumed, these results suggest that discontinuity thicknesses of less than about 5 km are required to reflect observable P waves at 1 Hz [e.g., *Richards*, 1972; *Lees et al.*, 1983], a constraint recently confirmed using synthetic seismogram modeling [*Benz and Vidale*, 1993]. A linear impedance gradient of thickness h will act as a low pass filter to reflected waves. At vertical incidence this filter is closely approximated by convolution with a boxcar function of width $t_w = 2h/v$, where t_w is the two-way travel time through the discontinuity and v is the wave velocity (see Figure 5). The frequency response is given by a sinc function, the first zero of which occurs at $f_0 = 1/t_w$. We then have $h = v/2f_0 = \lambda/2$, where λ is the wavelength; the reflection coefficient becomes very small as the discontinuity thickness approaches half the wavelength.

However, some energy will be reflected at frequencies above f_0 (due to the effect of the "corners" in the velocity profile), so isolated observations of very high frequency reflections could occur, if focusing effects are invoked to boost the amplitudes to anomalous levels. Interpretation of $P'P'$ precursor results is further complicated by the likely presence of non-linear velocity increases, as predicted by models of mineral phase

changes [e.g., *Helffrich and Bina*, 1994; *Solomatov and Stevenson*, 1994; *Helffrich and Wood*, 1996; *Stixrude*, 1997]. The reflected pulse shape (assuming a delta function input) will mimic the shape of the impedance profile (Figure 5). In the frequency domain, the highest frequency reflections are determined more by the sharpness of the steepest part of the profile than by the total layer thickness. In principle, resolving the exact shape of the impedance profile is possible, given broadband data of sufficient quality. However, the effects of noise, attenuation and band-limited signals make this a challenging task. Recently, *Xu et al.* [1999] analyzed $P'P'$ observations at several short-period arrays and found that the *410* reflection could be best modeled as a 5-km-thick gradient region immediately above a sharp discontinuity.

The sharpness of the *660* has also been constrained by observations of high-frequency P-to-SV converted waves [e.g., *Paulssen*, 1988]; the *410* sharpness has been studied by analyzing precritical reflections from the triplications [e.g., *Vidale et al.*, 1995; *Neele*, 1996; *Melbourne and Helmberger*, 1998]. These results further support the evidence from $P'P'$ precursor observations that a large fraction of the total impedance increases for the *410* and *660* discontinuities occurs over depth intervals of ~5 km or less. A puzzling exception to this consensus is the analysis of P-to-SV converted phases of *Petersen et al.* [1993], who modeled the *660* as a linear gradient zone 20 to 30 km thick in order to explain pulse broadening observed in $P660s$. It should be noted that the *410* is observed less consistently than the *660* in $P'P'$ precursors, suggesting that the *410* may be more variable in sharpness and/or amplitude than the *660* [e.g., *Xu et al.*, 1998]. The absence of a *520* reflector in high-frequency $P'P'$ precursor observations [*Benz and Vidale*, 1993], combined with clear *520* reflectors in long-period SS precursor data, indicates that the 520-km "discontinuity" is between 10 and 50 km in thickness.

6. DISCONTINUITY AMPLITUDES

While the globally averaged discontinuity depths are now known to an accuracy approaching 1%, the size of the velocity and density increases at the discontinuities are known much more poorly. This results from the ambiguities in modeling seismic refraction data (discussed above), and from the fact that the amplitudes of discontinuity phases typically exhibit much more scatter than their travel times. Improving the reliability of estimates of discontinuity amplitudes is an important goal because seismic velocity profiles are widely used by mineral physicists to model their results and the discontinuity density contrasts provide a valuable constraint on geodynamic modeling of mantle flow.

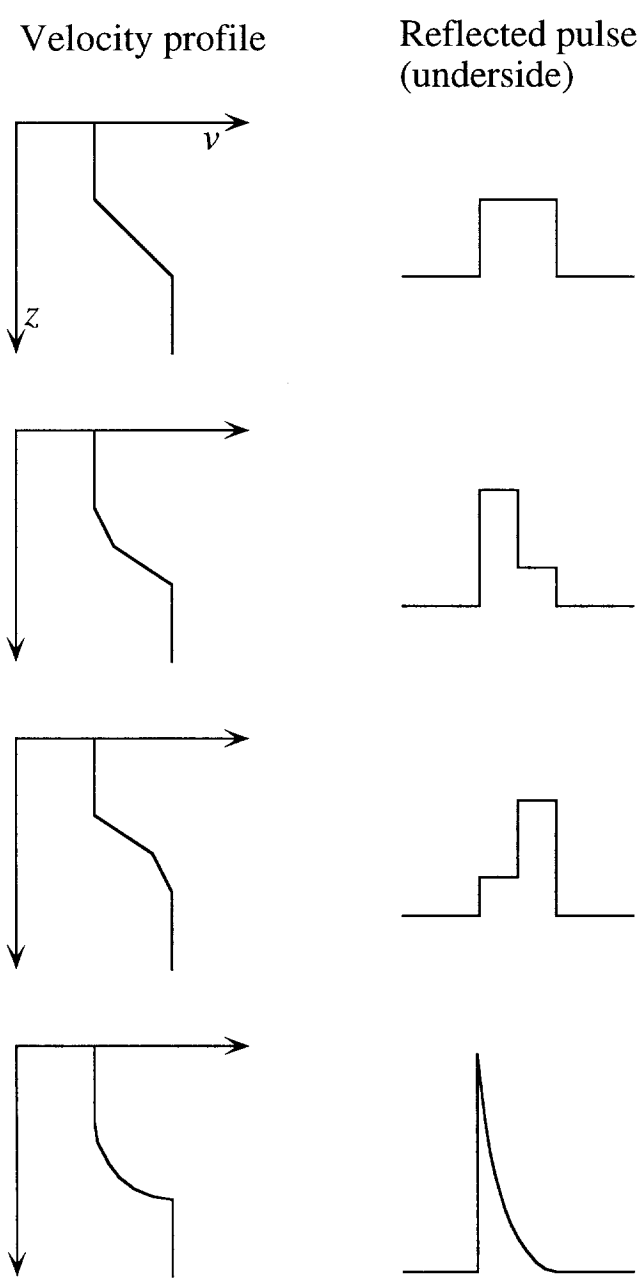

Figure 5. Cartoon of sharpness profiles and predicted reflected pulses resulting from underside discontinuity reflections.

Velocity models of the upper mantle for different regions (derived primarily from refraction data) have been

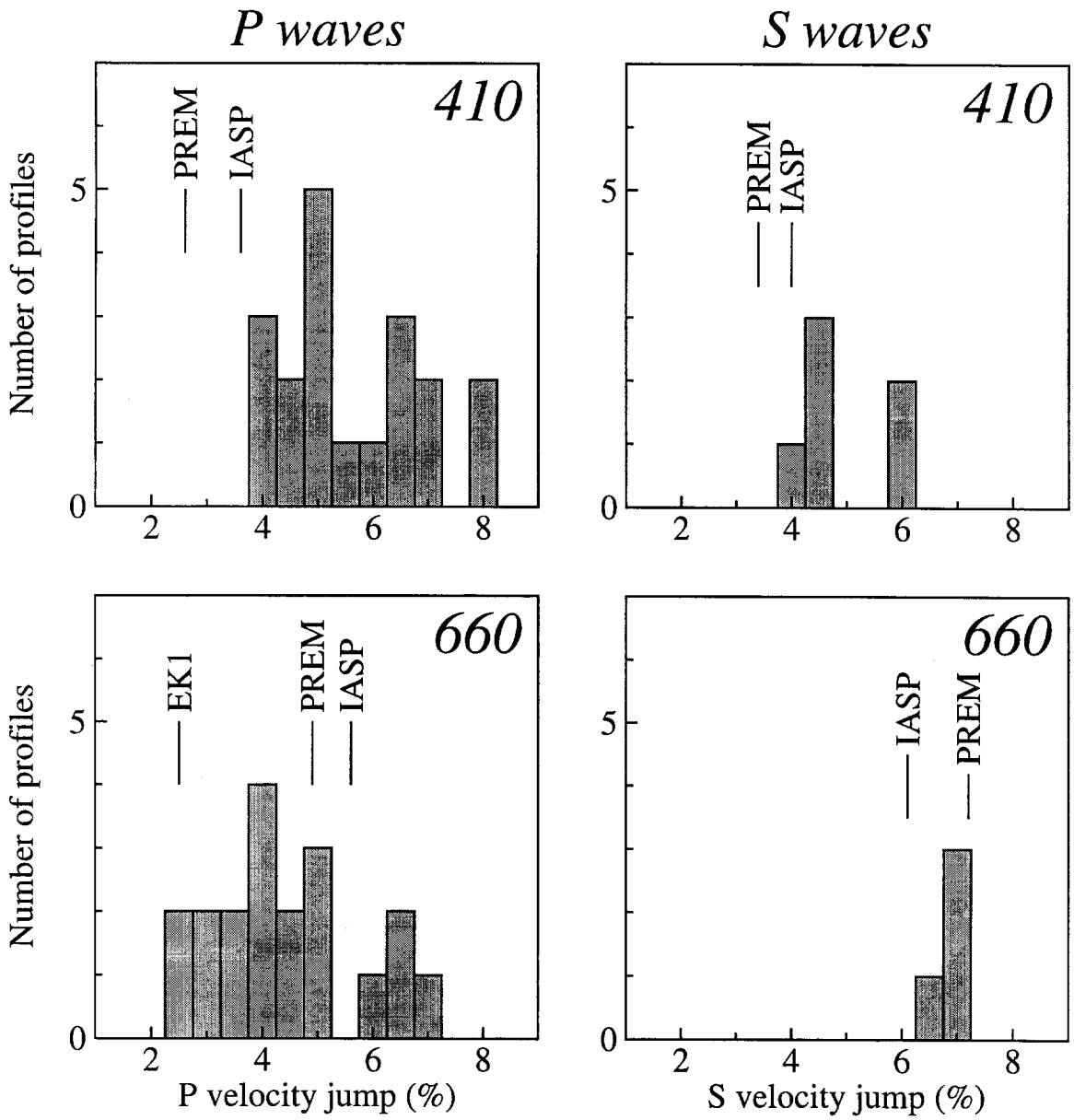

Figure 6. A histogram of P and S velocity jumps across the *410* and *660* discontinuities in published models cited by *Nolet and Wortel* [1989] and *Nolet et al.* [1994]. For reference, the PREM and IASP91 velocity jumps are also shown, as well as the recent model, EK1, proposed by *Estabrook and Kind* [1996] for the 660-km discontinuity.

summarized by *Nolet and Wortel* [1989] and *Nolet et al.* [1994]. The P velocity jumps at the *410* and *660* discontinuities from 19 different P velocity profiles are plotted in Figure 6. The P velocity increases vary from 4% to 8% (relative to the mean velocity) at the *410* and from 2.5% to 7% at the *660*. Average velocity jumps are 5.5% at the *410* and 4.5% at the *660*. Most of the profiles are derived from short-period data; the five profiles obtained from long-period or broadband data exhibit less scatter and have average P velocity jumps near 4.5% at both the *410* and *660* discontinuities. For comparison, the *410* and *660* P velocity jumps are 2.6% and 4.9% in the PREM model, 3.6% and 5.6% in the IASP91 model.

S velocity profiles are less common than P profiles (see Figure 6). Profiles derived from long-period or broadband data have a mean S velocity jump of 4.9%

at the *410* (from 6 profiles) and 6.8% at the *660* (from 4 profiles). However, this consensus is somewhat misleading because three of the profiles (SNA, TNA, NWA) were constructed with identical velocity profiles through the transition zone. For comparison, the *410* and *660* S velocity jumps are 3.4% and 7.2% in the PREM model [*Dziewonski and Anderson*, 1981], 4.0% and 6.1% in the IASP91 model [*Kennett*, 1991].

Clearly there is considerable scatter in these observations, particularly for the P velocities. It is interesting that the PREM and IASP91 models do not necessarily represent a consensus of the available data. Compared to the average profile, both models have smaller P velocity jumps at the *410* and larger P velocity jumps at the *660*. The PREM P velocity change of 2.6% at the *410* is particularly anomalous; it is about half the average change in the other models. However, since most of the individual profiles are from continental regions, they may not represent a reasonable global average.

The density increases at the discontinuities are known less reliably than the velocities, since they are generally inferred using velocity versus density scaling relationships. Normal mode frequencies provide constraints on density but with poor radial resolution compared to seismic velocity profiles inferred from body wave travel times. *Kennett* [1998] identified a range of density profiles that satisfy a subset of the normal mode data; permitted density jumps at the *410* and *660* vary by over a factor of two. The PREM density jumps are 5.0% at the *410* and 9.3% at the *660* (the IASP91 model does not specify density). The bulk of the density profiles produced by *Kennett* [1998] contain larger density changes than PREM at the *410* and smaller changes at the *660*, although the PREM model is consistent with the data.

Secondary seismic phases resulting from topside and bottomside reflections off the discontinuities are generally sensitive to the impedance jump at the interfaces. The PREM S impedance jumps are 8% at the *410* and 16% at the *660*. From analysis of ScS reverberations, *Revenaugh and Jordan* [1991a] obtained S impedance contrast estimates of 9.2% and 14.4% for the *410* and *660*, respectively. Using stacks of SS precursors with oceanic bouncepoints, *Shearer* [1996] obtained values of 6.7% at the *410* and 9.9% at the *660*. In both of these studies, uncertainties in the corrections applied to account for incoherent stacking effects limit the accuracy of the estimates. More reliable is the 410/660 impedance ratio, which varies between 0.64 and 0.68 in the two studies. This agreement strongly suggests that the PREM 410/660 S impedance ratio of 0.5 is too small.

In principle, the S velocity jumps at the discontinuities could be obtained from the amplitudes of P-to-SV converted phases. In contrast to the reflected phases, these arrivals are relatively insensitive to the discontinuity density contrasts. However, studies of P-to-SV conversions have mainly focused on the timing of the arrivals and analysis of the amplitudes has been limited. *Shearer* [1991] obtained a value of 0.86 ± 0.17 for the $P410s/P660s$ amplitude ratio, but, given the scatter in the data, did not estimate a corresponding value for the S velocity jumps at the discontinuities.

A few years ago, *Estabrook and Kind* [1996] analyzed long-period PP precursors and concluded, based on the absence of an observable $P660P$ phase, that the P velocity contrast at the *660* is only about 2.5%. This is a surprising result, as this value is substantially less than most previous models, and, if confirmed, would have important implications. It is not clear if such a small P velocity jump can be easily reconciled with the other available data sets, such as details of the observed *660* triplication in P travel times and the strong reflections from the *660* seen in $P'P'$ precursors. Such a small velocity contrast would also require significant adjustments to the velocity gradients above and below the *660* discontinuity. However, it should also be noted that the EK1 model proposed by *Estabrook and Kind* [1996] appears no more anomalous with respect to published *660* models than the PREM and IASP91 models are with respect to published *410* models (see Figure 6). Recently, *Shearer and Flanagan* [1999] analyzed both SS and PP precursor amplitudes and found that a range of models (including PREM) could fit the observed $S410S$ and $P410P$ amplitudes, but that the EK1 model provided a much better fit than PREM to the 660-km amplitudes. Their analysis suggests a relatively tight constraint on the density jump at 660 km, with values ranging from 4 to 6%, significantly less than the PREM value of 9.3%. The Shearer and Flanagan study supports the conclusion of *Gaherty et al.* [1999] that a pyrolite model fits the seismic properties of the 410-km discontinuity, but suggests a mismatch between the observed *660* properties and the pyrolite model of *Weidner and Wang* [1998].

Little is yet known about possible lateral variations in the discontinuity amplitudes. *Revenaugh and Jordan* [1991a], in their ScS reverberation work, noted a correlation between the S reflection coefficient and the apparent depth of the *660* discontinuity, with the reflection coefficient becoming smaller as the discontinuity becomes deeper. However, *Shearer* [1991] could not resolve a correlation in SS precursor data between re-

flector amplitude and depth for either the *410* or *660* discontinuities. Some indication that the *410* is more variable in amplitude and/or sharpness than the *660* is provided by the $P'P'$ precursor studies, which sometimes image the *660* and not the *410*, but never vice versa [e.g., *Xu et al.*, 1998].

The size of the *520* discontinuity has been resolved by only a few studies. The 520-km reflectors seen in the *ScS* reverberation analysis of *Revenaugh and Jordan* [1991a] suggest an S impedance increase of 2.8–4.0%. The SS precursor study of *Shearer* [1996] indicates an S impedance change of 2.2–3.6%. *Ryberg et al.* [1997] examined three long-range refraction profiles across Siberia and estimated that the P velocity increase across the *520* is 0.25 ± 0.05 km/s (a 2.5% increase). However, the lack of *520* observations in other refraction data [notably *Cummins et al.*, 1992; *Jones et al.*, 1992] suggests that the *520* may vary in strength between different regions, in which case the global average P velocity increase is likely to be less than 2.5%. *Gu and Dziewonski* [1998] found evidence from SS precursor data that the *520* may be absent beneath continental shields; however, this conflicts with the *Ryberg et al.* [1997] evidence for a *520* beneath the Siberian shield. *Flanagan and Shearer* [1998a] argue that the *520* is most likely a global feature, which is not always clearly observed in SS precursor data due to signal-to-noise problems.

7. DISCUSSION

While the properties of the upper mantle discontinuities can be studied simply in the interest of improving seismic models of Earth structure, they also have important implications for mineral physics and geodyamics. At one time, many researchers believed that the *660* discontinuity marked a compositional change between the upper and lower mantle that divided convection in the mantle into two separate flow regimes. However, it is now widely recognized that the *660* is largely, if not entirely, a result of phase changes in mantle minerals. Nonetheless, the negative Clapeyron slope of the γ-spinel to perovskite + magnesiowüstite phase change near 660 km suggests that the *660* will act to inhibit thermally driven flow across the interface. However, from instantaneous flow calculations based on density structures inferred from mantle tomography results, it appears that the observed large-scale topography on the *660* is insufficient to prevent whole mantle flow [e.g., *Phipps Morgan and Shearer*, 1993].

Topography on the *660* gives rise to lateral density anomalies due to the density increase across the boundary. These density differences cause buoyancy forces that strongly affect mantle flow. Because of this, the *660* provides a convenient place for geodynamic modelers to place structure so that their flow models fit geophysical constraints such as the geoid or dynamic topography [e.g., *Thoraval et al.*, 1995], or to force layered convection [e.g., *Forte and Woodward*, 1997]. The importance of the SS precursor analyses is that they provide direct observational constraints on the amplitude and pattern of this topography [e.g., see Plate 1). Models of topography on the transition zone discontinuities are likely to continue to improve as more seismic data are analyzed. An important step will be to perform joint inversions of discontinuity phase data (such as SS precursor times) with mantle tomography data sets to produce unified models of discontinuity topography and three-dimensional velocity variations [e.g., *Gu and Dziewonski*, 1997], and to use back-projection techniques [e.g., *Shearer et al.*, 1999] to improve model resolution compared to the common-midpoint stacking approaches that have generally been used thus far.

With the *660* phase change appearing unlikely to prevent whole mantle convection, attention recently has focused on the possibility of an additional mantle discontinuity that might be the true barrier to mantle flow. *Jeanloz* [1991] hypothesized the existence of a small density increase across a compositional interface (which might or might not coincide with the position of the 660-km discontinuity). Depending upon the size of the accompanying velocity change and the amplitude of the topography on the interface, this feature might be very hard to detect through seismic observations. The difficulty in reconciling predicted dynamic topography with surface observations has also led to hypothesized discontinuities at other depths. *Ravine and Phipps Morgan* [1996] achieved superior fits in their modeling when a discontinuity was introduced at the base of the asthenosphere (~300 km depth), while *Wen and Anderson* [1997] found that a barrier at about 900 km depth could improve their modeling results. Based on an inferred minimum in a heat flow model, *Forte and Woodward* [1997] proposed that mantle properties might change near 1000 km. Recently, *Kellogg et al.* [1999] hypothesized that a compositional boundary may exist near 1600 km depth.

However, direct seismic observations to support these ideas are as yet inconclusive. Evidence has sometimes been found for discontinuities near 900 km depth [e.g., *Petersen et al.*, 1993; *Kawakatsu and Niu*, 1994] and these studies can be compelling for at least the local existence of anomalous structures. However, observations from different subduction zones [*Niu and Kawakatsu*,

1997] suggest depths varying from 900 to 1080 km for this feature, and other studies have identified discontinuities at a wide variety of additional depths in the upper mantle. It is unclear how many of these observations could represent the same interface at different depths; the uniqueness of a 900-km interface is uncertain. If such a feature exists, it is likely to be characterized by very large topographic variations so that it is sufficiently globally incoherent as to remain invisible in stacks of long-period seismograms. Large dynamic topography is predicted by flow calculations if only a small density contrast exists across the discontinuity.

While the depths to the transition zone discontinuities are being resolved with increasing accuracy, constraints on the size of the velocity and density increases at the *410* and *660* remain distressingly poor. In particular, estimates of the globally averaged P velocity increases near 410 and 660 km are scattered by more than a factor of two (see Figure 6). This is key area for seismologists to improve their observations, since P velocity depth profiles are widely used by mineral physicists to model their results. More definitive numbers for the velocity jumps would help in resolving the continuing controversy over the fraction of olivine present in the mantle.

A possible wild card is the increasing evidence for widespread compositional variability in the mantle [e.g., *van der Hilst and Karason*, 1999; *Kaneshima and Helffrich*, 1999]. Such heterogeneity is indicated at very small scales (~8 km) in the lower mantle from PKP precursor observations [*Hedlin et al.*, 1997], and may be required in the transition zone to explain observed small-scale (~200 km) discontinuity topography [e.g., *Dueker and Sheehan*, 1997]. Significant compositional heterogeneity would greatly complicate modeling of mantle processes, as observed seismic velocity heterogeneity and discontinuity topography could no longer be used in any simple way to infer temperature and density variations.

Acknowledgments. This work was supported by National Science Foundation grant EAR96-14350.

REFERENCES

Adams, R.D., Reflections from discontinuities beneath Antarctica, *Bull. Seismol. Soc. Am.*, *61*, 1441–1451, 1971.

Barley, B.J., J.A. Hudson, and A. Douglas, S to P scattering at the 650 km discontinuity, *Geophys. J. R. Astron. Soc.*, *69*, 159–172, 1982.

Baumgardt, D.R., and S.S. Alexander, Structure of the mantle beneath Montana LASA from analysis of long-period mode-converted phases, *Bull. Seismol. Soc. Am.*, *74*, 1683–1702, 1984.

Benz, H.M., and J.E. Vidale, Sharpness of upper-mantle discontinuities determined from high-frequency reflections, *Nature*, *365*, 147–150, 1993.

Bina, C.R. and G. Helffrich, Phase transition Clapeyron slopes and transition zone seismic discontinuity topography, *J. Geophys. Res.*, *99*, 15,853–15,860, 1994.

Bock, G., *Sp* phases from the Australian upper mantle, *Geophys. J.*, *94*, 73–81, 1988.

Bock, G., Synthetic seismogram images of upper mantle structure: No evidence for a 520-km discontinuity, *J. Geophys. Res.*, *99*, 15,843–15,851, 1994.

Bock, G., and J. Ha, Short-period S–P conversion in the mantle at a depth near 700 km, *Geophys. J. R. Astron. Soc.*, *77*, 593–615, 1984.

Bock, G., and R. Kind, A global study of S-to-P and P-to-S conversions from the upper mantle transition zone, *Geophys. J. Int.*, *107*, 117–129, 1991.

Bostock, M.G., *Ps* conversions from the upper mantle transition zone beneath the Canadian landmass, *J. Geophys. Res.*, *101*, 8393–8402, 1996.

Brudzinski, M.R., W.-P. Chen, R.L. Nowack, and B.-S. Huang, Variations of P wave speeds in the mantle transition zone beneath the northern Philippine Sea, *J. Geophys. Res.*, *102*, 11,815–11,827, 1997.

Castle, J.C., and K.C. Creager, Seismic evidence against a mantle chemical discontinuity near 660 km depth beneath Izu-Bonin, *Geophys. Res. Lett.*, *24*, 241–244, 1997.

Castle, J.C., and K.C. Creager, Topography of the 660-km seismic discontinuity beneath Izu-Bonin: Implications for tectonic history and slab deformation, *J. Geophys. Res.*, *103*, 12,511–12,527, 1998.

Castle, J.C., and K.C. Creager, A steeply dipping discontinuity in the lower mantle beneath Izu-Bonin, *J. Geophys. Res.*, *104*, 7279–7292, 1999.

Chaljub, E., and A. Tarantola, Sensitivity of SS precursors to topography on the upper-mantle 660-km discontinuity, *Geophys. Res. Lett.*, *24*, 2613–2616, 1997.

Chen, Y.H., S.W. Roecker, and G.L. Kosarev, Elevation of the 410 km discontinuity beneath the central Tien Shan: Evidence for a detached lithospheric root, *Geophys. Res. Lett.*, *24*, 1531–1534, 1997.

Collier, J.D., and G. Helffrich, Topography of the "410" and "660" km seismic discontinuities in the Izu-Bonin subduction zone, *Geophys. Res. Lett.*, *24*, 1535–1538, 1997.

Cummins, P.R., B.L.N. Kennett, J.R. Bowman, and M.G. Bostock, The 520-km discontinuity, *Bull. Seismol. Soc. Am.*, *82*, 323-336, 1992.

Davis, J.P., R. Kind, and I.S. Sacks, Precursors to $P'P'$ re-examined using broad-band data, *Geophys. J. Int.*, *99*, 595–604, 1989.

Dey-Sarkar, S.K., and R.A. Wiggins, Upper mantle structure in western Canada, *J. Geophys. Res.*, *81*, 3619–3632, 1976.

Drummond, B.J., K.J. Muirhead, and A.L. Hales, Evidence for a seismic discontinuity near 200 km depth under a continental margin, *Geophys. J. R. Astron. Soc.*, *70*, 67–77, 1982.

Dueker, K.G., and A.F. Sheehan, Mantle discontinuity structure from midpoint stacks of converted P to S waves across the Yellowstone hotspot track, *J. Geophys. Res.*, *102*, 8313–8327, 1997.

Dueker, K.G., and A.F. Sheehan, Mantle discontinuity

structure beneath the Colorado Rocky Mountains and High Plains, *J. Geophys. Res., 103*, 7153–7169, 1998.

Dziewonski, A.M., and D.L. Anderson, Preliminary reference Earth model, *Phys. Earth Planet. Inter., 25*, 297–356, 1981.

Engdahl, E.R., and E.A. Flinn, Seismic waves reflected from discontinuities within earth's upper mantle, *Science, 163*, 177–179, 1969.

Estabrook, C.H., G. Bock, and R. Kind, Investigation of mantle discontinuities from a single deep earthquake, *Geophys. Res. Lett., 21*, 1495–1498, 1994.

Estabrook, C.H., and R. Kind, The nature of the 660-km upper-mantle seismic discontinuity from precursors to the *PP* phase, *Science, 274*, 1179–1182, 1996.

Faber, S., and G. Müller, *Sp* phases from the transition zone between the upper and lower mantle, *Bull. Seismol. Soc. Am., 70*, 487–508, 1980.

Faber, S., and G. Müller, Converted phases from the mantle transition zone observed at European stations, *J. Geophys., 54*, 183–194, 1984.

Flanagan, M.P., and P.M. Shearer, Global mapping of topography on transition zone discontinuities by stacking SS precursors, *J. Geophys. Res., 103*, 2673–2692, 1998a.

Flanagan, M.P., and P.M. Shearer, Topography on the 410-km seismic velocity discontinuity near subduction zones from stacking of *sS*, *sP*, and *pP* precursors, *J. Geophys. Res., 103*, 21,165–21,182, 1998b.

Flanagan, M.P., and P.M. Shearer, A map of topography on the 410-km discontinuity from PP precursors, *Geophys. Res. Lett., 26*, 549–552, 1999.

Forte, A.M., and R.L. Woodward, Seismic-geodynamic constraints on three-dimensional structure, vertical flow, and heat transfer in the mantle, *J. Geophys. Res., 102*, 17,981–17,994, 1997.

Fukao, Y., Upper mantle *P* structure on the ocean side of the Japan-Kurile arc, *Geophys. J. R. Astron. Soc., 50*, 621–642, 1977.

Fukao, Y., M. Obayashi, H. Inoue, and M. Nenbai, Subducting slabs stagnant in the mantle transition zone, *J. Geophys. Res., 97*, 4809–4822, 1992.

Gaherty, J.B., Y. Wang, T.H. Jordan and D.J. Weidner, Testing plausible upper-mantle compositions using fine-scale models of the 410-km discontinuity, *Geophys. Res. Lett., 26*, 1641–1644, 1999.

Given, J.W., and D.V. Helmberger, Upper mantle structure of northwestern Eurasia, *J. Geophys. Res., 85*, 7183–7194, 1980.

Gossler, J., and R. Kind, Seismic evidence for very deep roots of continents, *Earth Planet. Sci. Lett., 138*, 1–13, 1995.

Grand, S.P., and D.V. Helmberger, Upper mantle shear structure of North America, *Geophys. J. R. Astron. Soc., 76*, 399–438, 1984.

Graves, R.W., and D.V. Helmberger, Upper mantle cross section from Tonga to Newfoundland, *J. Geophys. Res., 93*, 4701–4711, 1988.

Gu, Y., A.M. Dziewonski, and W. Su, Joint inversion for mantle structure and topography of upper mantle discontinuities using B-splines, *EOS Trans. AGU (Fall meeting suppl.), 78*, F484, 1997.

Gu, Y., and A.M. Dziewonski, Global de-correlation of the topography of transition zone discontinuities, *Earth Planet. Sci. Lett., 157*, 57–67, 1998.

Gurrola, H., *Investigation of the upper mantle transition zone through velocity spectrum stacking of receiver functions*, Ph.D. thesis, University of California, San Diego, 1995.

Gutowski, P.R., and E.R. Kanasewich, Velocity spectral evidence of upper mantle discontinuities, *Geophys. J. R. Astron. Soc., 36*, 21–32, 1974.

Hales, A.L., A seismic discontinuity in the lithosphere, *Earth Planet. Sci. Lett., 7*, 44–46, 1969.

Hales, A.L., K.J. Muirhead, and J.M.W. Rynn, A compressional velocity distribution for the upper mantle, *Tectonophysics, 63*, 309–348, 1980.

Hedlin, M.A.H., P.M Shearer, and P.S. Earle, Seismic evidence for small-scale heterogeneity throughout the Earth's mantle, *Nature, 387*, 145–150, 1997.

Helffrich, G., and C.R. Bina, Frequency dependence of the visibility and depths of mantle seismic discontinuities, *Geophys. Res. Lett., 21*, 2613–2616, 1994.

Helffrich, G., and B. Wood, 410-km discontinuity sharpness and the form of the olivine α–β phase diagram: resolution of apparent seismic contradictions, *Geophys. J. Int., 126*, F7–F12, 1996.

Helmberger, D.V., and G.R. Engen, Upper mantle shear structure, *J. Geophys. Res., 79*, 4017–4028, 1974.

Helmberger, D.V., and R.A. Wiggins, Upper mantle structure of midwestern United States, *J. Geophys. Res., 76*, 3229–3245, 1971.

Husebye, E.S., R.A.W. Haddon, and D.W. King, Precursors to $P'P'$ and upper mantle discontinuities, *J. Geophys., 43*, 535–543, 1977.

Iidaka, T., and D. Suetsugu, Seismological evidence for metastable olivine inside a subducting slab, *Nature, 356*, 593–595, 1992.

Jeanloz, R., Effects of phase transitions and possible compositional changes on the seismological structure near 650 km depth, *Geophys. Res. Lett., 18*, 1743–1746, 1991.

Johnson, L.R., Array measurements of *P* velocities in the upper mantle, *J. Geophys. Res., 72*, 6309–6325, 1967.

Jones, L.E., J. Mori, and D.V. Helmberger, Short-period constraints on the proposed transition zone discontinuity, *J. Geophys. Res., 97*, 8765–8774, 1992.

Kaneshima, S., and G. Helffrich, Detection of lower mantle scatterers northeast of the Marianna subduction zone using short-period array data, *J. Geophys. Res., 103*, 4825–4838, 1998.

Kaneshima, S., and G. Helffrich, Dipping low-velocity layer in the mid-lower mantle: evidence for geochemical heterogeneity, *Science, 283*, 1888–1891, 1999.

Katzman, R., L. Zhao, and T.H. Jordan, High-resolution, 2D vertical tomography of the central Pacific mantle using *ScS* reverberations and frequency-dependent travel times, *J. Geophys. Res., 103*, 17,933–17,971, 1998.

Kawakatsu, H., and F. Niu, Seismic evidence for a 920-km discontinuity in the mantle, *Nature, 371*, 301–305, 1994.

Kellogg, L.H., B.H. Hager, and R.D. van der Hilst, Compositional stratification in the deep mantle, *Science, 283*, 1881–1884, 1999.

Kennett, B.L.N., editor, *IASPEI 1991 Seismological Tables*, Research School of Earth Sciences, Australian National University, Canberra, 1991.

Kennett, B.L.N., On the density distribution within the Earth, *Geophys. J. Int.*, *132*, 374–382, 1998.

Kind, R., and L.P. Vinnik, The upper-mantle discontinuities underneath the GRF array from *P*-to-*S* converted phases, *J. Geophys.*, *62*, 138–147, 1988.

Kirby, S.H., S. Stein, E.A. Okal, and D.C. Rubie, Metastable mantle phase transformations and deep earthquakes in subducting oceanic lithosphere, *Rev. Geophys.*, *34*, 261–306, 1996.

Kosarev, G., R. Kind, S.V. Sobolev, X. Yuan, W. Hanka, and S. Oreshin, Seismic evidence for a detached Indian lithospheric mantle beneath Tibet, *Science*, *283*, 1306–1309, 1999.

Le Stunff, Y., C.W. Wicks, and B. Romanowicz, $P'P'$ precursors under Africa: evidence for mid-mantle reflectors, *Science*, *270*, 74–77, 1995.

Lee, D.-K., and S.P. Grand, Depth of the upper mantle discontinuities beneath the East Pacific Rise, *Geophys. Res. Lett.*, *23*, 3369–3372, 1996.

Lees, A.C, M.S.T. Bukowinski, and R. Jeanloz, Reflection properties of phase transition and compositional change models of the 670-km discontinuity, *J. Geophys. Res.*, *88*, 8145–8159, 1983.

LeFevre, L.V., and D.V. Helmberger, Upper mantle *P* velocity structure of the Canadian shield, *J. Geophys. Res.*, *94*, 17749–17765, 1989.

Leven, J.H., I. Jackson, and A.E. Ringwood, Upper mantle seismic anisotropy and lithospheric decoupling, *Nature*, *289*, 234–239, 1981.

Li, A., K.M. Fischer, T.J. Clarke, M.E. Wysession, M.J. Fouch, and G.I. Al-Eqabi, Mantle discontinuities beneath eastern North America, *EOS Trans. AGU (Fall Meeting Suppl.)*, *77*, F474, 1996.

Li, A., K.M. Fischer, M.E. Wysession, and T.J. Clarke, Mantle discontinuities and temperature under the North American continental keel, *Nature*, *395*, 160–163, 1998.

Mechie, J., A.V. Egorkin, K. Fuchs, T. Ryberg, L. Solodilov, and F. Wenzel, P-wave mantle velocity structure beneath northern Eurasia from long-range recordings along the profile Quartz, *Phys. Earth Planet. Inter.*, *79*, 269-286, 1993.

Melbourne, T, and D. Helmberger, Fine structure of the 410 km discontinuity, *J. Geophys. Res.*, *103*, 10,091–10,102, 1998.

Nakanishi, I., Seismic reflections from the upper mantle discontinuities beneath the Mid-Atlantic ridge observed by a seismic array in Hokkaido region, Japan, *Geophys. Res. Lett.*, *13*, 1458–1461, 1986.

Nakanishi, I., Reflections of $P'P'$ from upper mantle discontinuities beneath the Mid-Atlantic Ridge, *Geophys. J.*, *93*, 335–346, 1988.

Nakanishi, I., A search for topography of the mantle discontinuities from precursors to $P'P'$, *J. Phys. Earth*, *37*, 297–301, 1989.

Neele, F., Sharp 400-km discontinuity from short-period *P* reflections, *Geophys. Res. Lett.*, *23*, 419–422, 1996.

Neele, F., H. de Regt, and J. VanDecar, Gross errors in upper-mantle discontinuity topography from underside reflection data, *Geophys. J. Int.*, *129*, 194–204, 1997.

Niazi, M., The use of source arrays in studies of regional structure, *Bull. Seismol. Soc. Am.*, *59*, 1631–1643, 1969.

Niazi, M., and D.L. Anderson, Upper mantle structure of western North America from apparent velocities of *P* waves, *J. Geophys. Res.*, *70*, 4633–4640, 1965.

Niu, F., and H. Kawakatsu, Direct evidence for the undulation of the 660-km discontinuity beneath Tonga: comparison of Japan and California array data, *Geophys. Res. Lett.*, *22*, 531–534, 1995.

Niu, F., and H. Kawakatsu, Depth variation of the mid-mantle seismic discontinuity, *Geophys. Res. Lett.*, *24*, 429–432, 1997.

Nolet, G., The upper mantle under western Europe inferred from the dispersion of Rayleigh modes, *J. Geophys.*, *43*, 265–285, 1977.

Nolet, G., S.P. Grand, and B.L.N. Kennett, Seismic heterogeneity in the upper mantle, *J. Geophys. Res.*, *99*, 23,753–23,766, 1994.

Nolet, G., and M.J.R. Wortel, Mantle, upper: structure, in *The Encyclopedia of Solid Earth Geophysics*, edited by D.E. James, pp. 775–788, Van Nostrand Reinhold, New York, 1989.

Paulssen, H., Upper mantle converted waves beneath the NARS array, *Geophys. Res. Lett.*, *12*, 709–712, 1985.

Paulssen, H., Evidence for a sharp 670-km discontinuity as inferred from *P*-to-*S* converted waves, *J. Geophys. Res.*, *93*, 10489–10500, 1988.

Petersen, N., J. Gossler, R. Kind, K. Stammler, and L. Vinnik, Precursors to *SS* and structure of transition zone of the north-western Pacific, *Geophys. Res. Lett.*, *20*, 281–284, 1993.

Petersen, N., L. Vinnik, G. Kosarev, R. Kind, S. Oreshin, and K. Stammler, Sharpness of the mantle discontinuities, *Geophys. Res. Lett.*, *20*, 859–862, 1993.

Phipps Morgan, J., and P.M. Shearer, Seismic constraints on mantle flow and topography of the 660-km discontinuity: evidence for whole mantle convection, *Nature*, *365*, 506–511, 1993.

Pino, N.A., and D.V. Helmberger, Upper mantle compressional velocity structure beneath the West Mediterranean Basin, *J. Geophys. Res.*, *102*, 2953–2967, 1997.

Ram, A., and R.F. Mereu, Lateral variations in upper-mantle structure around India as obtained from Gauribidanur seismic array data, *Geophys. J. R. Astron. Soc.*, *49*, 87–113, 1977.

Ravine, M.A., and J. Phipps Morgan, Inversion for radial mantle viscosity with a layered flow constraint: a better fit to dynamic topography?, *EOS Trans. AGU (Fall meeting suppl.)*, *77*, F721, 1996.

Revenaugh, J., and T.H. Jordan, Observations of first-order mantle reverberations, *Bull. Seismol. Soc. Am.*, *77*, 1704–1717, 1987.

Revenaugh, J., and T.H. Jordan, A study of mantle layering beneath the western Pacific, *J. Geophys. Res.*, *94*, 5787–5813, 1989.

Revenaugh, J., and T.H. Jordan, Mantle layering from *ScS* reverberations: 2. the transition zone, *J. Geophys. Res.*, *96*, 19763–19780, 1991a.

Revenaugh, J., and T.H. Jordan, Mantle layering from *ScS* reverberations: 3. the upper mantle, *J. Geophys. Res.*, *96*, 19781–19810, 1991b.

Revenaugh, J., and T.H. Jordan, Reply, *J. Geophys. Res.*, *97*, 19,549–19,551, 1992.

Revenaugh, J., and S.A. Sipkin, Mantle discontinuity struc-

ture beneath China, *J. Geophys. Res.*, *99*, 21,911–21,927, 1994.

Richards, P.G., Seismic waves reflected from velocity gradient anomalies within the Earth's upper mantle, *J. Geophys.*, *38*, 517–527, 1972.

Richards, M.A., and C.W. Wicks, *S–P* conversion from the transition zone beneath Tonga and the nature of the 670 km discontinuity, *Geophys. J. Int.*, *101*, 1-35, 1990.

Rigden, S.M., G.D. Gwanmesia, J.D. FitzGerald, I. Jackson, and R.C. Liebermann, Spinel elasticity and seismic structure of the transition zone of the mantle, *Nature*, *354*, 143–145, 1991.

Ritsema, J., M. Hagerty, and T. Lay, Comparison of broad-band and short-period seismic wave-form stacks—implications for upper-mantle discontinuity structure, *Geophys. Res. Lett.*, *22*, 3151–3154, 1995.

Ryberg, T., F. Wenzel, A.V. Egorkin, K. Fuchs, and L. Solodilov, Two-dimensional velocity structure beneath northern Eurasia derived from the super long-range seismic profile Quartz, *Bull. Seismol. Soc. Am.*, *86*, 857–867, 1996.

Ryberg, T., F. Wenzel, A.V. Egorkin, and L. Solodilov, Short-period observation of the 520 km discontinuity in northern Eurasia, *J. Geophys. Res.*, *102*, 5413–5422, 1997.

Ryberg, T., F. Wenzel, A.V. Egorkin, and L. Solodilov, Properties of the mantle transition zone in northern Eurasia, *J. Geophys. Res.*, *103*, 811-822, 1998.

Sacks, I.S., J.A. Snoke, and E.S. Husebye, Lithosphere thickness beneath the Baltic Shield, *Tectonophysics*, *56*, 101–110, 1979.

Shearer, P.M., Seismic imaging of upper-mantle structure with new evidence for a 520-km discontinuity, *Nature*, *344*, 121–126, 1990.

Shearer, P.M., Constraints on upper mantle discontinuities from observations of long-period reflected and converted phases, *J. Geophys. Res.*, *96*, 18,147–18,182, 1991.

Shearer, P.M., Global mapping of upper mantle reflectors from long-period *SS* precursors, *Geophys. J. Int.*, *115*, 878–904, 1993.

Shearer, P.M., Transition zone velocity gradients and the 520-km discontinuity, *J. Geophys. Res.*, *101*, 3053–3066, 1996.

Shearer, P.M., and M.P. Flanagan, Seismic velocity and density jumps across the 410- and 660-kilometer discontinuities, *Science*, *285*, 1545–1548, 1999.

Shearer, P.M., M.P. Flanagan, and M. Hedlin, Experiments in migration processing of *SS* precursor observations to image upper-mantle discontinuity structure, *J. Geophys. Res.*, *104*, 7229–7242, 1999.

Shearer, P.M., and T.G. Masters, Global mapping of topography on the 660-km discontinuity, *Nature*, *355*, 791–796, 1992.

Shen, Y., A.F. Sheehan, K.G. Dueker, C. de Groot-Hedlin, H. Gilbert, Mantle discontinuity structure beneath the southern East Pacific Rise from P-to-S converted phases, *Science*, *280*, 1232–1235, 1998.

Shen, Y., S.C. Solomon, I.T. Bjarnason, and G.M. Purdy, Hot mantle transition zone beneath Iceland and the adjacent Mid-Atlantic Ridge inferred from P-to-S conversions and the 410- and 660-km discontinuities, *Geophys. Res. Lett.*, *23*, 3527–3530, 1996.

Shen, Y., S.C. Solomon, I.T. Bjarnason, and C.J. Wolfe, Seismic evidence for a lower-mantle origin of the Iceland plume, *Nature*, *395*, 62–65, 1998.

Simpson, D.W., R.F. Mereu, and D.W. King, An array study of *P*-wave velocities in the upper mantle transition zone beneath northeastern Australia, *Bull. Seismol. Soc. Am.*, *64*, 1757–1788, 1974.

Solomatov, V., and D.J. Stevenson, Can sharp seismic discontinuities be caused by non-equilibrium phase transformations?, *Earth Planet. Sci. Lett.*, *125*, 267–279, 1994.

Souriau, A., First analyses of broadband records on the Geoscope network: potential for detailed studies of mantle discontinuities, *Geophys. Res. Lett.*, *13*, 1011–1014, 1986.

Stammler, K., and R. Kind, Comment on "Mantle layering from *ScS* reverberations, 2, The transition zone" by J. Revenaugh and T.H. Jordan, *J. Geophys. Res.*, *97*, 17,547–17,548, 1992.

Stammler, K., R. Kind, G.L. Kosarev, A. Plesinger, J. Horalek, L. Qiyuan, and L.P. Vinnnik, Broadband observations of *PS* conversions from the upper mantle in Eurasia, *Geophys. J. Int.*, *105*, 801–804, 1991.

Stammler, K., R. Kind, N. Petersen, G. Kosarev, L. Vinnnik, and L. Qiyuan, The upper mantle discontinuities: correlated or anticorrelated?, *Geophys. Res. Lett.*, *19*, 1563–1566, 1992.

Stixrude, L., Structure and sharpness of phase transitions and mantle discontinuities, *J. Geophys. Res.*, *102*, 14,835–14,852, 1997.

Thoraval, C., P. Machetel, and A. Cazenave, Locally layered convection inferred from dynamic models of the Earth's mantle, *Nature*, *375*, 777–780, 1995.

van der Hilst, R., R. Engdahl, W. Spakman, and G. Nolet, Tomographic imaging of subducted lithosphere below northwest Pacific island arcs, *Nature*, *353*, 37–43, 1991.

van der Hilst, R.D., and H. Karason, Compositional heterogeneity in the bottom 1000 kilometers of Earth's mantle: toward a hybrid convection model, *Science*, *283*, 1885–1888, 1999.

van der Lee, S., H. Paulssen, and G. Nolet, Variability of *P*660*s* phases as a consequence of topography of the 660 km discontinuity, *Phys. Earth Planet. Inter.*, *86*, 147–164, 1994.

Vidale, J.E. and H.M. Benz, Upper-mantle seismic discontinuities and the thermal structure of subduction zones, *Nature*, *356*, 678–683, 1992.

Vidale, J.E., X.Y. Ding, and S.P. Grand, The 410-km-depth discontinuity: a sharpness estimate from near-critical reflections, *Geophys. Res. Lett.*, *22*, 2557–2560, 1995.

Vinnik, L.P., Detection of waves converted from *P* to *SV* in the mantle, *Phys. Earth Planet. Inter.*, *15*, 39–45, 1977.

Vinnik, L.P., R.A. Avetisjan, and N.G. Mikhailova, Heterogeneities in the mantle transition zone from observations of *P*-to-*SV* converted waves, *Phys. Earth Planet. Inter.*, *33*, 149–163, 1983.

Vinnik, G. Kosarev, and N. Petersen, Mantle transition zone beneath Eurasia, *Geophys. Res. Lett.*, *23*, 1485–1488, 1996.

Walck, M.C., The *P*-wave upper mantle structure beneath an active spreading centre: the Gulf of California, *Geophys. J. R. Astron. Soc.*, *76*, 697–723, 1984.

Wallace, T.C. and W.E. Holt, The 670 km discontinuity and

precursors to $P'P'$: implications for the sharpness of the boundary and its global extent, *EOS Trans. AGU, 69*, 1333, 1988.

Wen, L., and D.L. Anderson, Layered mantle convection: a model for geoid and topography, *Earth Planet. Sci. Lett., 146*, 367–377, 1997.

Whitcomb, J.H., and D.L. Anderson, Reflection of $P'P'$ seismic waves from discontinuities in the mantle, *J. Geophys. Res., 75*, 5713–5728, 1970.

Wicks, C.W., and M.A. Richards, A detailed map of the 660-kilometer discontinuity beneath the Izu-Bonin subduction zone, *Science, 261*, 1424–1427, 1993.

Wiggins, R.A., and D.V. Helmberger, Upper mantle structure of the western United States, *J. Geophys. Res., 78*, 1870–1880, 1973.

Xu, F., J.E. Vidale, P.S. Earle, and H.M. Benz, Mantle discontinuities under southern Africa from precursors to $P'P'_{df}$, *Geophys. Res. Lett., 25*, 571–574, 1998.

Xu, F., P.S. Earle and J.E. Vidale, Survey of precursors to $P'P'$: Constraints on mantle discontinuities, *EOS Trans. AGU (Fall Meeting Supplement)*, in press, 1999.

Yamazaki, A., and K. Hirahara, The thickness of upper mantle discontinuities, as inferred from short-period J-Array data, *Geophys. Res. Lett., 21*, 1811–1814, 1994.

Weidner, D.J. and Y. Wang, Chemical and Clapeyron-induced buoyancy at the 660-km discontinuity, *J. Geophys. Res., 103*, 7431–7441, 1998.

Zhang, Z., and T. Lay, Investigation of upper mantle discontinuities near northwestern Pacific subduction zones using precursors to *sSH*, *J. Geophys. Res., 98*, 4389–4405, 1993.

Zhao, L.-S., and D.V. Helmberger, Upper mantle compressional velocity structure beneath the northwest Atlantic Ocean, *J. Geophys. Res., 98*, 14,185–14,196, 1993.

P. Shearer, IGPP 0225, U.C. San Diego, La Jolla, CA 92093-0225. (e-mail: pshearer@ucsd.edu)